Available online at www.sciencedirect.com

jmr&t
Journal of Materials Research and Technology

journal homepage: www.elsevier.com/locate/jmrt

Original Article

Martensitic transformation, microstructure and functional behavior of thin-walled Nitinol produced by micro laser metal wire deposition

Carlo Alberto Biffi [a,*], *Ausonio Tuissi* [a], *Ali Gökhan Demir* [b]

[a] *National Research Council, CNR ICMATE, Institute of Condensed Matter Chemistry and Technologies for Energy, Via Previati 1, Lecco, 23900, Italy*

[b] *Department of Mechanical Engineering, Politecnico di Milano, Via La Masa 1, Milan, 20156, Italy*

ARTICLE INFO

Article history:
Received 27 November 2020
Accepted 29 March 2021
Available online 4 April 2021

Keywords:
Additive manufacturing
Nitinol
Microstructure
Martensitic transformation
Directed energy deposition

ABSTRACT

Additive manufacturing (AM) of Nitinol could enable realizing smart 3D metallic structures that combine the functional properties of shape memory alloys with higher geometrical flexibility. However, powder feedstocks suffer from issues related to availability, chemical composition stability, and long-term stocking. Therefore, wire-based AM processes are considered promising for reducing the time required for the process development stage and for maintaining quality over time. In this study, micro laser metal wire deposition (μLMWD) was used for manufacturing thin walls with heights of up to 40 mm by using commercial superelastic Nitinol wires of 0.4 mm diameter. The microstructure, martensitic transformation (MT), and mechanical behavior were analyzed. The results showed that μLMWD could be used to produce Nitinol walls with high aspect ratio and sub-millimeter thickness, that were free of cracks and produced with relative density as high as 99%. The as-deposited wall section was characterized by an almost homogenous composition, which was associated with a solubilized condition, owing to the multiple heating cycles during the deposition of advancing layers. Limited amount of Ni loss induced an increase in the characteristic temperatures of the MT, and shape memory behavior was detected with a recoverable strain of 4.4% upon heating up to 120 °C.

1. Introduction

Additive manufacturing (AM) has opened up new possibilities for the product design and development of shape memory alloy (SMA) devices. SMAs are functional materials that possess unique properties such as shape memory effect (SME) and pseudoelasticity (PE) [1]. An intermetallic NiTi compound is the most widely used SMA owing to its stable and optimal functional performance. These two peculiar characteristics are due to a diffusionless solid-to-solid phase transformation, namely, the martensitic transformation (MT), that can be controlled above or below room temperatures by modifying

* Corresponding author.
E-mail address: carloalberto.biffi@cnr.it (C.A. Biffi).

https://doi.org/10.1016/j.jmrt.2021.03.108

the Ni content of the near-equiatomic NiTi phase within the stable compositional range [1]. Thus, the temperature range at which the MT occurs determines the use of NiTi mainly as an actuator or a biomedical device based on the shape memory effect or superelasticity, respectively.

Combined with the complex geometrical features obtainable with metal AM processes, the use of the shape memory effect could enable the fabrication of 4D materials, where the dimension of time is added to the material geometry. As NiTi alloys are one of the most widely studied SMAs, they have also been explored as materials for AM, mainly by employing powder feedstocks with powder bed fusion techniques such as selective laser melting (SLM), electron beam melting (EBM), and direct energy deposition (DED) [2–4]. These AM processes are characterized by high geometrical precision, ability to create internal channels, reasonable surface roughness, and capacity to produce lattice structures in materials [5–7]. However, compared with powder bed fusion techniques, DED processes such as laser metal deposition (LMD) have attracted less research attention [8,9].

The AM of Nitinol (an alloy of nickel and titanium) can be highly critical in terms of controlling the final Ni content in a built part, especially owing to the preferential vaporization of Ni [10]. This means that chemical variations can occur during the AM process, resulting in deviations from the initial chemical composition of the feedstock. The Ni loss during the AM process can result in issues with the final use of the component as well as process instabilities arising from the local differences in the shape memory behavior of the material. Therefore, the feedstock material should be carefully selected to potentially compensate for the Ni loss. In this regard, the production of powder feedstock via atomization can be cumbersome for controlling and maintaining the desired chemical composition within and among production batches. Such variations can be more critical for the NiTi alloy performance as it is highly sensitive to its chemical composition. Studies have investigated the element-wise mixing of powder and wire feedstocks for dealing with issues concerning chemical composition variations in DED processes [11,12]. While NiTi powder feedstocks are not yet highly consumed by AM end-users, thin NiTi wires are widely available in the market and are being developed for various applications. Commercial NiTi wires are available in different diameters and have significantly lower prices than that of powder feedstock having the same chemical composition. Different heat soruces, like electrical arc and plasma, were studied in DRD processes using NiTi wires [13–17].

Recently, the use of pulsed wave (PW) laser emission has been demonstrated to be effective for depositing wires of small diameters without significant enlargement of the track width compared to the wire diameter [18]. Micro laser metal wire deposition (μLMWD) can be a good approach for manufacturing small-scale 3D components or small-scale semi-finished parts (e.g., plate, tube, and ring) made of Nitinol. This process is intrinsically safer compared to powder deposition, and the feedstock dimensions are comparable to the diameters of commercially available NiTi wires (0.4–0.5 mm). The feasibility of the μLMWD process has been demonstrated for several materials such as stainless steel [18], $AlSi_{12}$ alloy [19], and Mg-alloy with Dy as the main alloying element [20]. PW laser emission with thin wires was proven to be effective in improving the dimensional precision to the range of that of powder-bed fusion processes [21]. These geometrical features make μLMWD ideal for manufacturing small parts or features in low volumes. Previous studies also showed that PW emission is effective in terms of limiting the material loss to only vaporization losses [18]. Moreover, the high material usage (laser efficiency) is beneficial for maintaining the chemical composition of the part with respect to its initial chemical composition.

The present study experimentally investigates the μLMWD processing of thin Nitinol wires having 0.4 mm diameter for producing thin-walled components. By using process conditions suitable for realizing multilayered deposition, the SMA properties were investigated with respect to the microstructure and chemical composition variations as well as the MT through optical and scanning electron microscopy methods, differential scanning calorimetry, and X-ray diffraction. The shape memory behavior was also detected via thermo-mechanical testing of the as-built wall. The results were analyzed by identifying the possibility of producing thin walls in Nitinol for reproducing functional parts when starting from commercial wires.

2. Experimental section

2.1. Material

Straight-annealed Nitinol (Ni50.8Ti49.2 at%, Saes Getters) wires with 0.4 mm diameter and a 5-mm-thick Ti6Al4V base plate were used throughout this study. The characteristic temperatures and transformation enthalpies of the Nitinol wire, as measured from the thermogram shown in Fig. 1, are listed in Table 1. The base plate alloy is characterized by sufficient weldability and metallurgical compatibility with NiTi alloys [6].

2.2. μLMWD process

The μLMWD setup used consisted of an automated laser welding station (Powerweld HL 124P, Trumpf, Ditzingen,

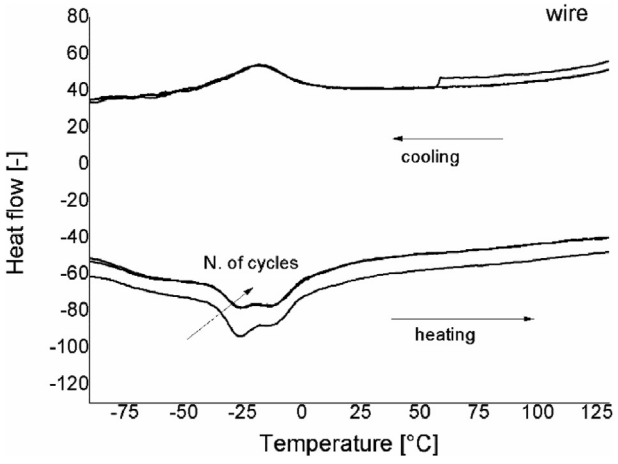

Fig. 1 – DSC scans of the initial Nitinol wire.

Table 1 – Characteristic temperatures and enthalpies of martensitic transformation, characteristic of the used Nitinol wire.

Characteristic features from DSC	Value
Martensite start temperature, M_s [°C]	3
Martensite finish temperature, M_f [°C]	−55
Austenite start temperature, A_s [°C]	−45
Austenite finish temperature, A_f [°C]	10
Enthalpy of austenite to martensite transformation, $H_{A\rightarrow M}$ [J/g]	3.5
Enthalpy of martensite to austenite transformation, $H_{M\rightarrow A}$ [J/g]	7.2

Germany) and the Lachesis custom-built wire feeding system, as shown in Fig. 2. A PW Nd:YAG laser source with a maximum average power of 120 W was used; it produced a maximum pulse energy (E) and peak power (P_{peak}) of 50 J and 5 kW, respectively. The output beam was coupled to a 0.4-mm-diameter delivery fiber that was collimated with a 200-mm-diameter lens and focused with a 150-mm-diameter lens. In this configuration, the minimum spot diameter obtained was 0.3 mm. The wire feeder was adjusted to control the wire angle, wire feed direction, and wire speed. The processing zone was protected with an inert gas layer provided through a shielding gas nozzle.

2.3. *Manufacturing of thin-walled NiTi structures*

In an initial phase, the process parameters were varied to determine a feasibility range for the stable melting of NiTi wires on single tracks. The laser spot size (d_s) was fixed at 0.65 mm to ensure a larger beam size compared to the wire diameter and to ensure that the wire tip remains under the beam despite variations in the wire position. The wire was fed frontally with a 30° inclination as this configuration has been found to maintain a stable process in previous studies [18–20]. The wire feed rate was fixed at 200 mm/min to provide stable wire insertion to the deposition zone. Ar (gas purity of 99.95%) was used as the local shielding gas. The process was found to be stable with pulse energies (E) of 6–6.8 J, pulse durations (τ) of 8.4–10 ms, and transverse speeds (v) of 90–110 mm/min. Within this feasibility range, the change in process parameters did not produce any significant changes in the track width and height, as shown in Fig. 3. The single tracks were found to be free of cracks and macropores. Hence, the central point of the feasibility window was chosen as a convenient combination of conditions for producing multilayered thin walls Here, E was 6.4 J, τ was 9.2 ms, and v was 100 mm/min. The corresponding peak and average powers were 695 W and 32 W, respectively. The average height and width of a single track obtained with these parameters was 251 ± 27 μm and 919 ± 35 μm, respectively. For the deposition of multilayered specimens, the height increment between the layers was set as 260 μm. Table 2 lists the final process parameters. Thin-walled specimens were produced by overlapping single-track layers over the build direction. No interlayer delay was applied between the layers except for the time required for the linear axis to move to the initial deposition point, which was ~3 s. The deposition length was 25 mm and 145 layers were deposited, thereby producing a nominal build height of 37.7 mm.

For analyses, the as-built samples were heat-treated in a furnace at 400 °C and 750 °C for 10 min in an inert atmosphere (Ar at 200 mbar) and then quenched in water, whereas the initial wire was heat-treated at 750 °C for 10 min.

2.4. *Sample characterization*

The part density was measured on the basis of Archimedes' principle using a Gibertini E50S2 precision digital balance and considering a full density of 6.45 g/cm^3. X-ray computed tomography (CT) was performed (Phoenix v|tome|x M 300, Baker Hughes) to characterize the types of defects occurring within the entire sample volume.

Metallographic analyses were conducted on the as-built samples as well as on the wire feedstock for comparison. Cross-sections of the built samples were taken over the build direction in the longitudinal and transversal directions

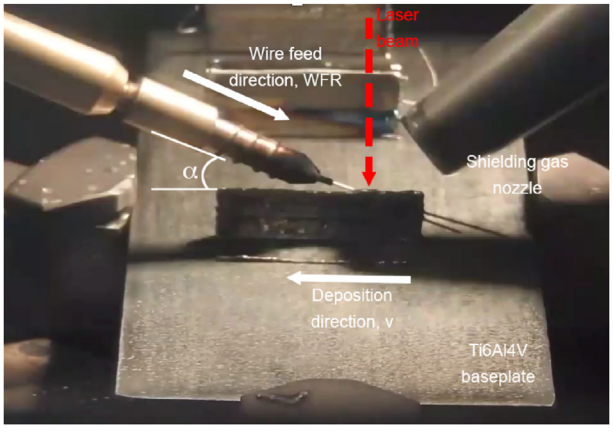

Fig. 2 – The main components of the LMWD system during the deposition of NiTi wires.

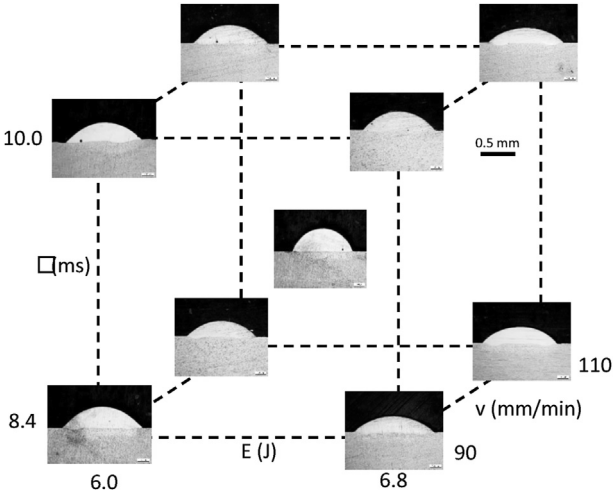

Fig. 3 – The influence of the main μLMWD process parameters on single track deposit geometry within the feasibility window.

Table 2 – Selected process parameters used in the experiments.

Process parameter	Value
Laser spot size, d_s (mm)	0.65 mm
Pulse repetition rate, PRR (Hz)	5 Hz
Wire feeding angle, α (°)	30
Wire feeding direction	Front
Wire feed rate, WFR (mm/min)	200 mm/min
Transverse speed, v (mm/min)	100 mm/min
Shielding gas	Ar at 1.4 bar
Pulse energy, E (J)	6.4 J
Pulse duration, τ (ms)	9.2 ms
Height increment, Δz (mm)	0.26 mm

relative to the deposition direction. Optical (Aristomet from Leitz, Oberkochen, Germany) and scanning electron microscopy (SEM, LEO 1413 from Zeiss, Oberocken, Germany) were performed for observing the melt pool geometry and microstructure. Moreover, compositional profiles were generated using energy-dispersive spectroscopy (EDS) along the build direction. MT was investigated using differential scanning calorimetry (DSC, DSC220C from Seiko, Tokyo, Japan). Samples with ~10 mg weight were extracted from the top, middle, and bottom positions of the built thin-walls. Five complete thermal cycles were conducted on each sample under a heating/cooling rate of 10 °C/min in the temperature range of 100 °C–150 °C. X-ray diffraction analysis (XRD, X'Pert PRO, Panalytical, Almelo, Netherlands) was performed on flat samples with dimensions of 8 mm × 8 mm × 0.8 mm for analyzing the martensitic and austenitic microstructures at low (−100 °C) and high (+120 °C) temperatures, respectively.

Thermomechanical testing was conducted in the tensile configuration on rectangular samples that were obtained by mechanical cutting from the central part of the deposited wall along the horizontal direction (xy, as shown in Fig. 4a; the sample size was 3 mm × 0.8 mm × 25 mm) using an MTS 2/M mechanical testing machine. A uniaxial tensile test was performed at 20 °C under crosshead control with a loading/unloading rate of 0.5%/min up to a maximum strain of 7%. After unloading, the samples were air-heated to 120 °C for evaluating the strain recovery.

3. Results and discussion

3.1. *Density and defect analysis*

Fig. 4b shows a sample of the Nitinol thin-walled structures produced by μLMWD. The layered structure is visible in the images. The relative density of the multi-layer structures was found to be 6.38 ± 0.01 g/cm^3 (98.9 ± 0.4% of the nominal density).

The main macro defects, namely, dripping and stubbing [22], visible on the material surface are typical ones in wire deposition processes. Stubbing occurs when insufficient energy is delivered to the wire, as a result of which the deposition follows an intermittent form. In μLMWD, stubbing can manifest in terms of small pieces of wire sticking out along the deposition direction. The process parameters were set to provide sufficient energy during the process. However, the misalignment of the wire tip with respect to the laser beam can cause partial irradiation of the wire. Such conditions occur towards the end of each layer and its frequency increases toward the top part of the thin-walled structures. During μLMWD, the melt pool solidifies between each laser pulse; therefore, constant contact is maintained throughout the process. The wire does not plunge into the melt pool, unlike what is common in wire deposition techniques that use arcs or continuous wave (CW) lasers [12,23]. While these conditions are certainly advantageous for maintaining small melt pool sizes and sub-millimeter thin wall dimensions, the process can become more susceptible to mechanical instabilities. By contrast, dripping occurs owing to high energy flux or thermal accumulation. The wire tip detaches from the deposition site and forms a large droplet that eventually falls on the workpiece owing to gravity [24]. However, such defects are not common in μLMWD because the PW laser emission is effective in avoiding such thermal accumulation.

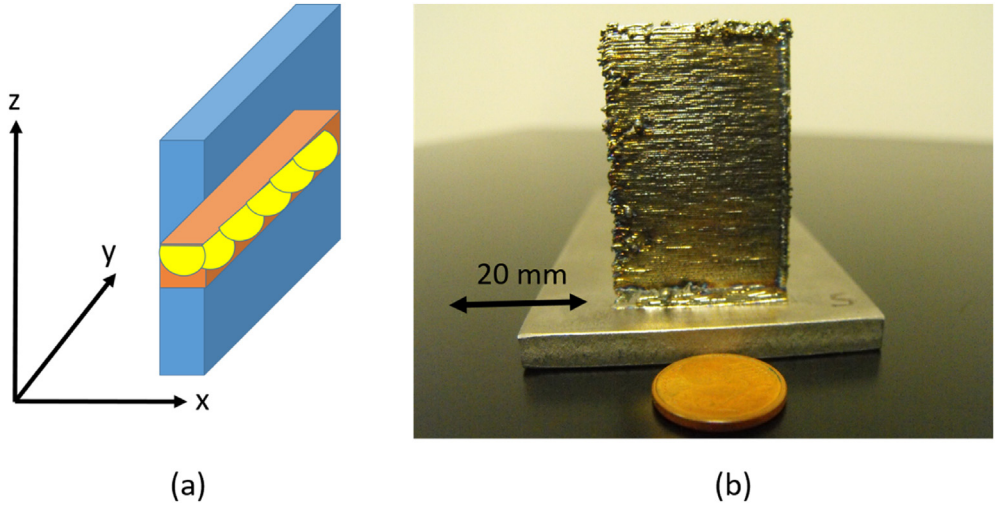

Fig. 4 – Schematic of the thin-walled structure (a) and a representative sample in Nitinol manufactured by μLMWD (b).

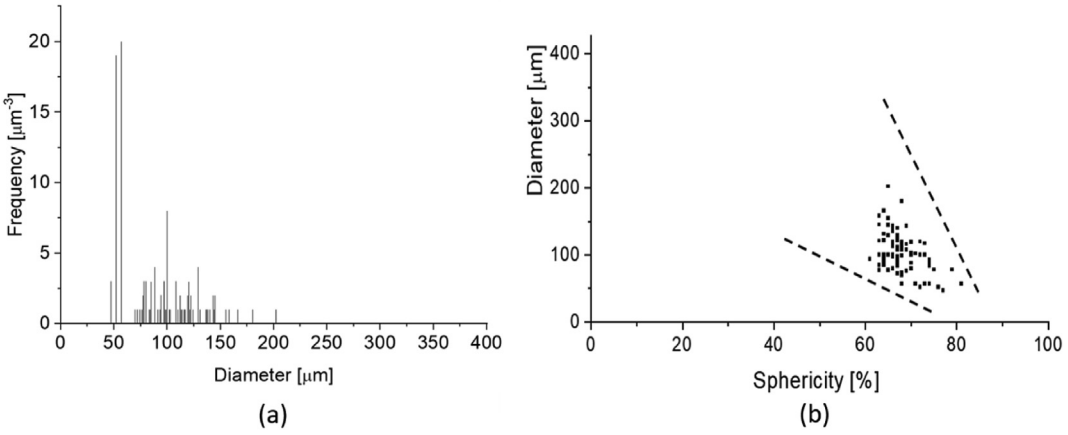

Fig. 5 – Defect diameter distribution (a) and diameter/sphericity trend (b) detected inside the thin-walled structure in Nitinol.

From the CT results shown in Fig. 5, it can be seen that the macro images and CT scans are coherent in terms of the defect formation mechanisms involved, which is related to the mechanical stability of the wire. However, the process evidently produces stable melt tracks, and the porosity disappears once mechanical stability is established. From the CT scans, an equivalent diameter was fitted to the pores found. Their deviations from a perfect sphere were assessed using the sphericity parameter, where a perfectly spherical pore would correspond to 100% sphericity. Fig. 5a shows that the defect sizes ranged from 50 to 200 μm. The highest defect frequency is associated with the lowest size, and a second peak corresponding to a defect with a size of ~100 μm was identified. The sphericities of the defects were also analyzed; Fig. 5b shows that the defect sphericity appears to be directly proportional to the diameter, and it increased from 60% up to 80% with a decrease in the defect size. The region of the defects highlighted in Fig. 5b could enable an in-depth analysis of the process conditions adopted during μLMWD. Here, most defects were characterized by high sphericities and average sizes lesser than the wire diameter. This region of the plot defect size vs. sphericity has already been identified in previous studies to indicate that the process was performed with sufficient energy for completely melting the Nitinol wire.

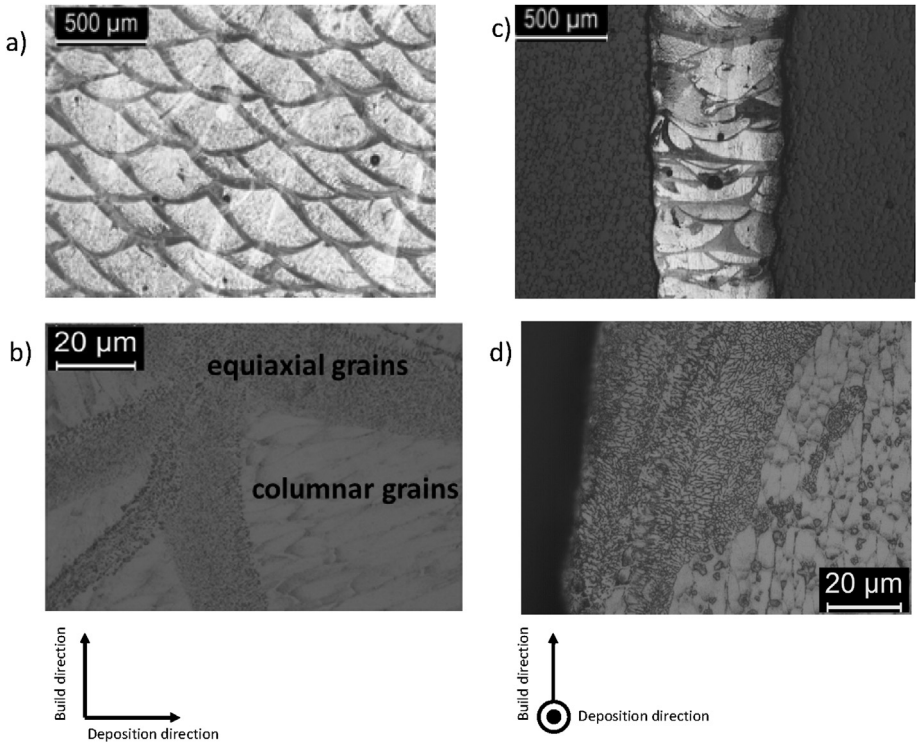

Fig. 6 – Microstructure of the Nitinol thin wall in longitudinal (a, b) and transverse (c, d) cross-sections, acquired at low and high magnifications.

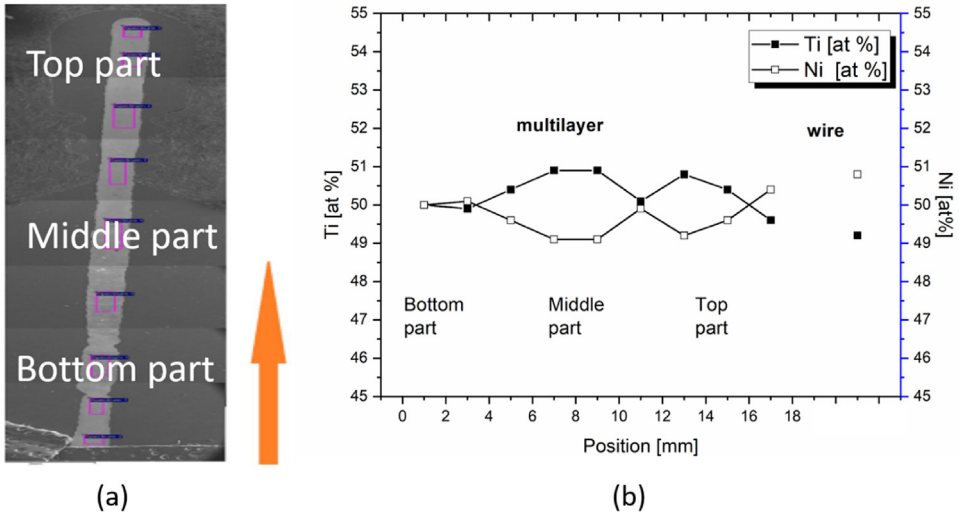

Fig. 7 – Compositional analysis done along the building direction: SEM image showing the cross section of the entire wall (a) and corresponding compositional profile (b). The arrow indicates the building direction.

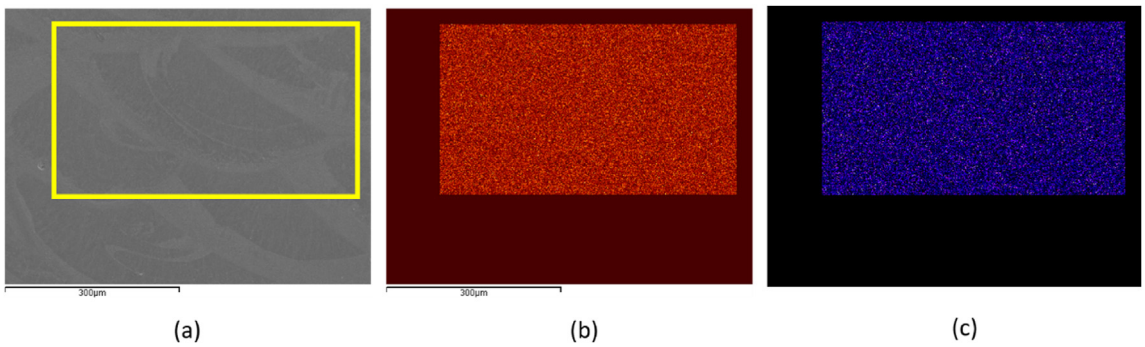

Fig. 8 – Chemical composition analysis performed via EDS map crossing a liquid pool: electron image picture (a), Ti (b) and Ni (c) elemental map.

Therefore, this confirms that the adopted condition was correctly selected for the realization of the thin-walled structures. In fact, Fiocchi et al. [20] noted that the lower right side of the porosity plot shown in Fig. 5b can be associated with the highest density.

3.2. *Microstructure and chemical composition*

Fig. 6 shows the longitudinal and transversal cross-sections acquired by optical microscopy at two selected magnifications. Fig. 6a and 6b shows the distribution of the melt pools in the longitudinal sections; these partially overlap each other owing to the layer-by-layer building strategy and the placement along the deposition direction. Columnar grains are detected in the semi-circular melt pool; these are oriented from the border to the center of the pool. In the transversal section, the microstructure indicates that solidification occurred preferentially along the X direction, and equiaxial grain growth was promoted owing to a slower cooling rate in the transverse plane than that in the longitudinal one (Fig. 6d). Moreover, the interphase regions among the melt pools on both planes exhibit the same microstructure.

Chemical composition analysis was performed along the build direction in the transverse section of the built wall. Fig. 7 shows the evolution of the Ti and Ni contents along the build

Table 3 – Average chemical compositions of the bottom, middle and top part of the as-built Nitinol wall, evaluated in the cross section (see Fig. 7a).

Region	Build height (mm)	Ti [at.%]	Ni [at.%]	Ni/Ti ratio
Top part	13–17	50.3 ± 0.6	49.7 ± 0.6	0.97
Middle part	7–11	50.6 ± 0.5	49.4 ± 0.5	0.99
Bottom part	1–5	50.1 ± 0.3	49.9 ± 0.3	1.00
Entire wall	0–20	50.3 ± 0.5	49.7 ± 0.5	0.99
Initial wire	–	49.2	50.8	1.03

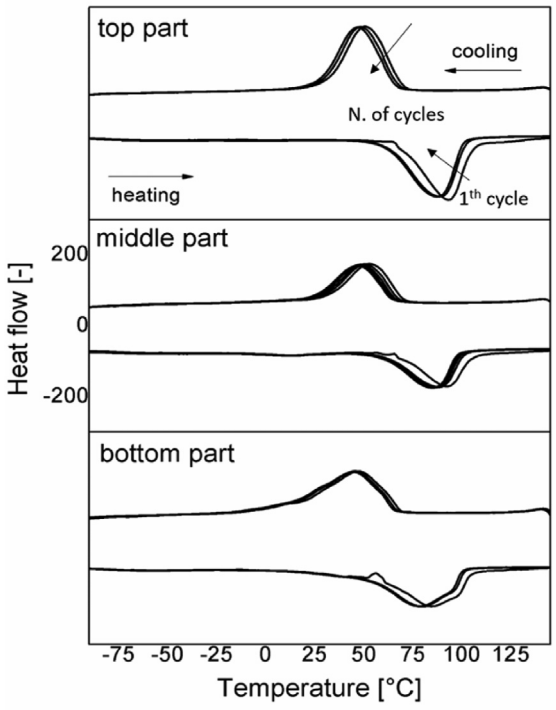

Fig. 9 – DSC scans of the top, middle and bottom region of the Nitinol thin-walled structure in the as-built condition.

direction along with that of the initial wire. The initial chemical composition is seen to vary significantly from the wire to the as-built wall. Ni loss is expected to occur preferentially during the partial evaporation caused by the laser beam [25,26]. The Ni:Ti ratio along the build direction was found to be uniform within the experimental error of 0.5 wt% of the measurement device. At higher magnifications, compositional analysis was performed within a single melt pool. Table 3 shows the average chemical compositions of the

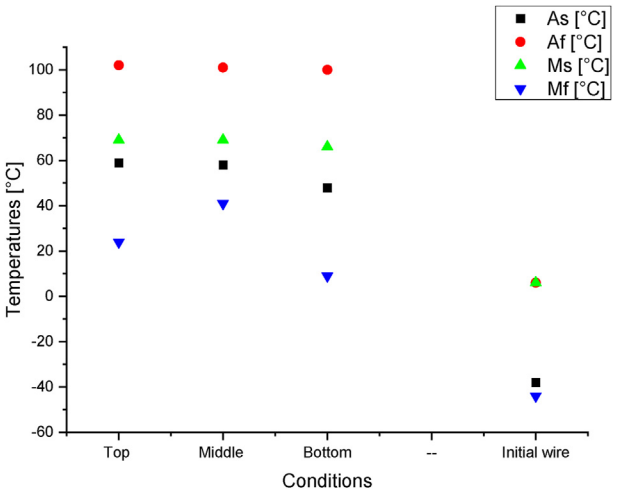

Fig. 10 – Temperatures of the MT, evaluated at the 2nd thermal cycle on the three regions of the thin-walled structure in as-built condition and the initial Nitinol wire.

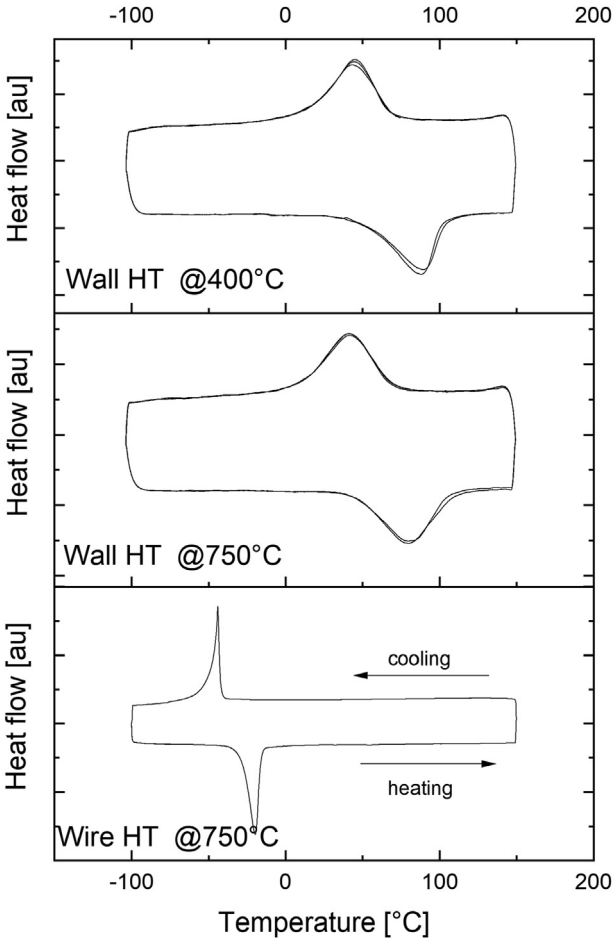

Fig. 11 – DSC scans of the Nitinol thin-walled structure after heat treatment carried out at 400 °C for 10 min (a) and at 750 °C for 10 min (b); DSC of the Nitinol wire after heat treatment at 750 °C for 10 min (c).

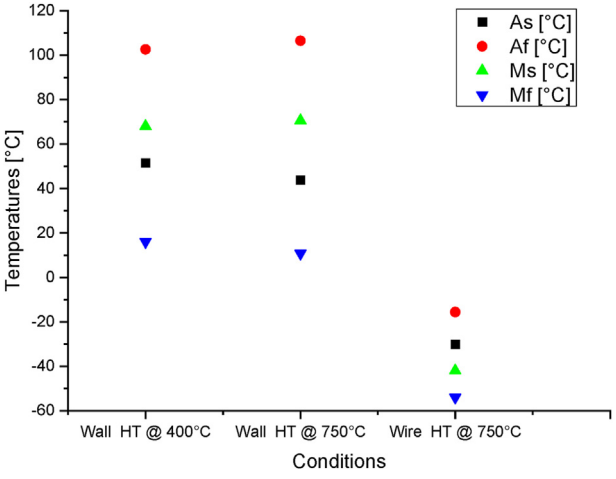

Fig. 12 – Temperatures of the MT, evaluated at the 2nd thermal cycle, of the Nitinol thin-walled structure after heat treatment carried out at 400 °C and at 750 °C for 10 min and the Nitinol wire after heat treatment at 750 °C for 10 min.

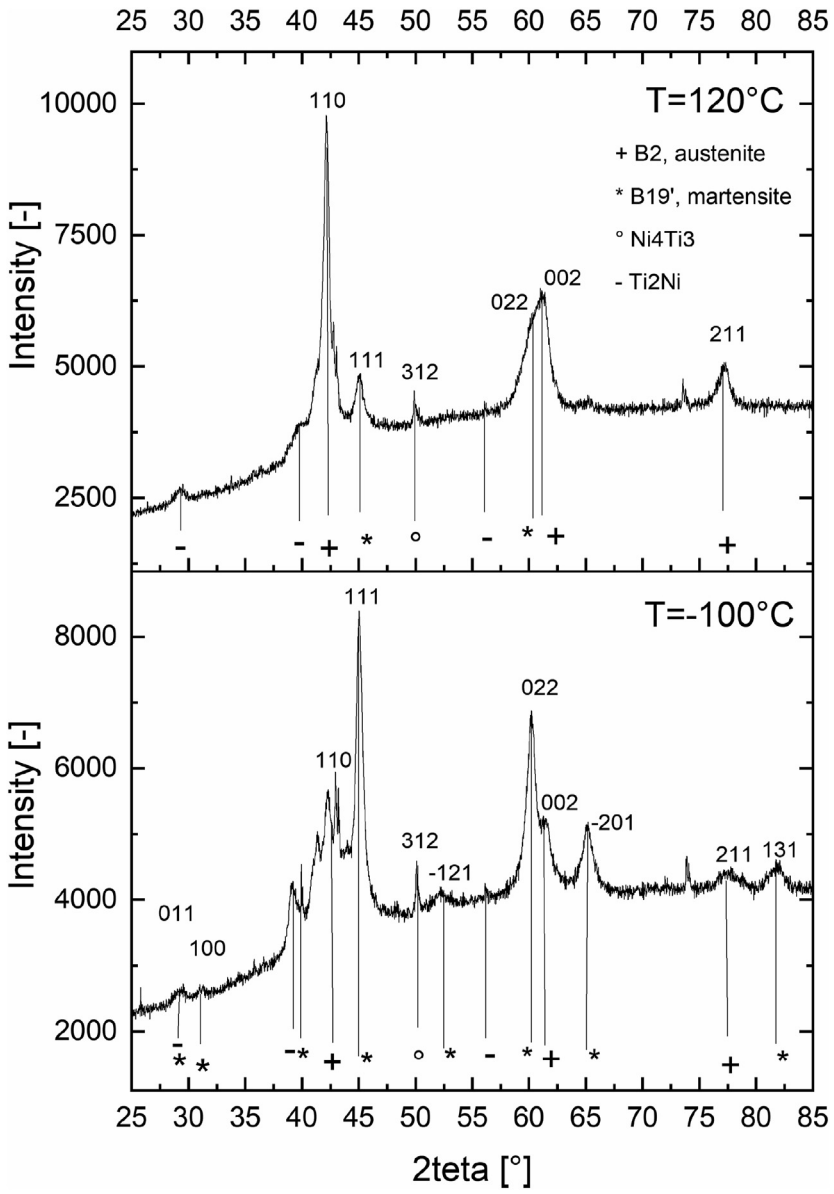

Fig. 13 – XRD patterns of the NiTi wall in as-built condition in the two extreme temperatures, at 120 °C and at −100 °C.

bottom, middle, and top regions of the of the melt pools. These results were compared with the total average value of the entire wall and the initial wire. The compositions measured in the three regions of the wall were found to overlap, thereby indicating good homogeneity of the Nitinol deposited during μLMWD. In contrast, the compositional analysis performed on the cross-section of the initial wire indicates a significant compositional change after μLMWD. In particular, the Ni content in the Nitinol wall decreased significantly from 50.8 at % to 49.7 at%. This induced a reduction in the Ni:Ti ratio with a consequent increase in the MT temperatures of the as-built material compared to the those of the initial wire. Even though the compositional change may appear very small, it can be enough to significantly change the functional performance of the NiTi compound [1,18]. Studies have already reported Ni loss in NiTi alloys during laser material processing. Owing to the high energy intensity, mainly with a Gaussian distribution, of the laser beam, high temperatures can be reached, especially at the center of the beam. Therefore, preferential evaporation of Ni may occur in the upper surface of the melt pool owing to its high vapor pressure [2].

Chemical composition analysis was also performed at higher magnifications to analyze the chemical homogeneity along the melt pools. Fig. 8a shows the EDS area, and Fig. 8b and c respectively show the compositional maps of elemental Ti and Ni. No evident elemental segregations were observed from the center to the border of the liquid pool, indicating that an almost constant Ni:Ti ratio was maintained. This homogeneity of the chemical composition can be explained by the laser–material interaction occurring in the long pulse duration domain (of the order of a few milliseconds) that allows the homogenization of the alloy without any significant segregation.

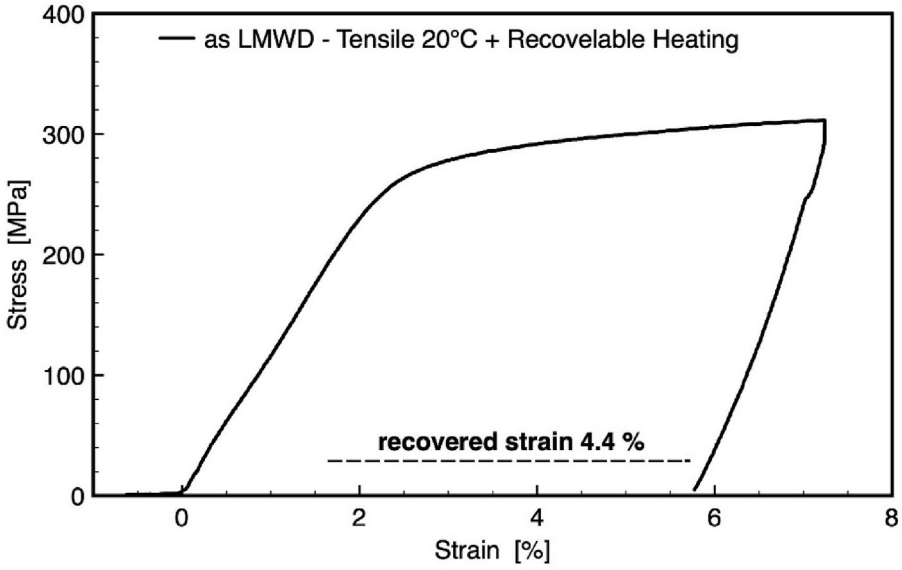

Fig. 14 – Tensile response of the NiTi thin-wall in as-built condition (XY orientation).

3.3. *Analysis of MT*

The top, middle, and bottom zones of the thin-walled structure were analyzed separately using DSC to study the MT behavior. Fig. 9 shows the DSC scans of three regions of the Nitinol wall in the as-built condition. Each sample was subjected to five complete thermal cycles to evaluate the thermal stability of the MT. A single-stage MT was detected after both heating and cooling in the thin-walled structure. No large variation in the MT temperatures from the top down to the bottom of the wall was seen. Moreover, the stability of the MT was maintained during the thermal cycles in the three regions of the wall. The DSC scans started to fully overlap from the second heating cycle, indicating that the alloy does not require any thermal cycling to stabilize the operating temperatures.

Fig. 10 shows the characteristic temperatures M_s and M_f (start and end of martensite formation on cooling, respectively) and A_s and A_f (start and end of austenite reformation on heating, respectively). The MT of the thin-walled structure was seen to exhibit a significantly different behavior with respect to the initial Nitinol wire. The results show that the wall produced by μLMWD exhibited a MT exceeding room temperature. For comparison, the initial wire was assumed to be superelastic because MT occurs below room temperature.

For a better understanding of the functional behavior of the Nitinol thin-walled structure, samples were subjected to stress relief at 400 °C and fully annealed at 750 °C for 10 min. For comparison, the initial wire was also fully annealed. Fig. 11 shows the DSC scans of the heat-treated Nitinol thin-walled structure and the Nitinol wire, and Fig. 12 shows the transformation temperatures of the MT.

The MT of the walled structure is seen to exhibit almost unvaried characteristic temperatures under the various conditions shown in Figs. 9 and 11. This suggests that during μLMWD, the as-built material does not accumulate residual stresses; it should be typically relaxed at a temperature of ~400 °C and it reaches a condition equivalent to at least that of a partially annealed alloy at 750 °C.

Accordingly, a comparison between the MT of the as-built thin-walled structure and that of the fully annealed wire can confirm Ni loss. The EDS is not satisfactorily precise for minimal variations of Ni. An increase in the transformation temperature can be associated with Ni loss of the order of 5 at % [1].

Fig. 13 shows the XRD patterns of the as-built Nitinol wall acquired at different temperatures. In particular, such patterns were detected above (120 °C, in austenite) and below the MT (−100 °C, in martensite) temperature. At 120 °C, the sample shows the principal peaks of the austenite B2, as indicated by the 110, 002, and 211 peaks; this agrees with the temperatures measured using DSC (see Fig. 9). Some martensite, possibly residual martensite, was also detected, as suggested from the 111 and 022 peaks. On the contrary, in the XRD pattern acquired at −100 °C, the principal peaks are associated with the formation of the martensite B19', as indicated by the 111 and 022 peaks. The residual austenite, characterized by a lower peak intensity, was also detected at temperatures below the MT temperature.

The analysis of the XRD patterns acquired at different temperatures reveals the presence of a Ni_4Ti_3 and Ti_2Ni phases having the similar intensities at both low and high temperatures. The presence of Ni_4Ti_3 can attributable to its precipitation during the cyclic heating and cooling experienced during the deposition of the successive layers. This secondary phase is typically obtained for heating at 400–500 °C for 30–60 min. The presence of Ti_2Ni phase can be confirmed by the Ni depletion from the matrix, as indicated by the EDS analysis, and by the increase in the MT temperatures,

as seen in the DSC scans. These results are in good agreement with those of similar wire AM processes [17].

Therefore, as noted in previous studies of the effects of MT temperatures on AM-produced NiTi parts [2], this change in material properties can be explained as follows:

(1) Change in Ni:Ti ratio: The chemical composition variation, previously detected from EDS analysis and then from DSC analysis, can result in the shift of the MT temperatures. Specifically, a lower Ni content in the alloy can be realized by increasing the characteristic temperatures [26].
(2) Precipitation: In NiTi SMAs, solution heat treatment is well known to promote the formation of precipitates such as Ni_4Ti_3 that reduce the Ni content in the matrix, and therefore, the MT temperatures can increase [25–28].
(3) Residual stresses: The rapid cooling rates associated with the layer-by-layer building strategy, which are inherent to the high cooling rate induced by laser melting, can promote the formation of residual stresses that tend to shift to higher temperatures in the MT. However, in this case, the fully annealed deposited Nitinol was found to exhibit a stress relieving effect.

It is worth mentioning that all these phenomena tend to work together, thereby producing complex effects on the MT [26]. Overall, the main contribution of this study is likely the finding of Ni loss during the process.

3.4. *Evaluation of the shape memory effect*

The thermomechanical behavior developed due to LMWD exhibits a typical shape memory effect, as shown in Fig. 14. From the DSC analysis shown in Figs. 9 and 10, the tensile specimen obtained from the middle part of the wall is characterized by an M_f of 40 °C and A_s of 58 °C; thus, this material is in a martensitic state at a testing temperature of 20 °C. Upon loading, after the initial elastic zone, detwinning of the martensite starts at ~250 MPa with an almost linear detwinning plateau up to a maximum strain of 7%. After unloading, a spring back effect was detectable, and a residual strain of 5.75% at 0 MPa was measured. The sample was heated to ~120 °C without applying any load, and a recoverable strain of 4.4% was measured (dashed line in Fig. 14). The materials fabricated by LMWD are not trained; therefore, a permanent deformation of 3.35% is seen after the first thermomechanical cycle.

4. Conclusions

In this study, micro laser metal wire deposition (μLMWD) was used for manufacturing thin walls with a height of up to 40 mm using a commercial superelastic Nitinol (Ni50.8Ti49.2 at%) wire. The following conclusions were drawn from this study:

- Nitinol walls with high aspect ratios and sub-millimeter thicknesses were obtained using the μLMWD process. They were free from cracks and had a relative density of ~99%.
- The material fabricated by μLMWD was characterized by a homogenous chemical composition in the entire wall section.
- The thin-walled structure showed MT with operating temperatures higher than those of the initial superelastic wire. This was due to a significant Ni loss of ~1 at% owing to the variation of the M_s temperature after heat-treatment was applied for realizing full annealing.
- The structure of the as-built condition was similar to that of a fully annealed alloy, probably owing to the cyclic heating through the advancing layers. Calorimetric analysis indicated the absence of any residual stresses in the as-built wall.
- Thermomechanical testing revealed shape memory behavior in the as-built sample, with a recoverable strain of 4.4% upon heating up to 120 °C.

It can be concluded that μLMWD can be successfully used for producing Nitinol components. The final shape memory or superelastic behavior is determined by the compositional variation during the process. The initial chemical composition of the wire feedstock should be carefully selected to compensate for the Ni loss to ensure the correct functioning of the device, including its superelastic and shape memory performances. The mechanical properties of the wire feedstock should also be considered for the process stability, which can vary with the transition from the superelastic to the shape memory region.

Declaration of Competing Interest

The authors wish to confirm that there are no known conflicts of interest associated with this publication.

Acknowledgments

Mr. Sherif Zaher Abbas Abdelaal and Mr. Jacopo Fiocchi are gratefully acknowledged for their support in the experimental activities. The authors would like to acknowledge Accordo Quadro CNR/Regione Lombardia n. 3866 at the 17/07/2015 FHfFC for the financial support. The Italian Ministry of Education, University and Research is also acknowledged for the support provided through the Project “Department of Excellence LIS4.0 - Lightweight and Smart Structures for Industry 4.0”.

REFERENCES

[1] Funakubo H. Shape memory alloys. Amsterdam: Gordon and Breach Science Publishers; 1987.
[2] Dadbakhsh S, Speirs M, Kruth JP, Schrooten J, Luyten J, Van Humbeeck J. Effect of SLM parameters on transformation temperatures of shape memory nickel titanium parts. Adv

Eng Mater 2014;16:1140–6. https://doi.org/10.1002/adem.201300558.
[3] Elahinia M, Shayesteh Moghaddam N, Taheri Andani M, Amerinatanzi A, Bimber BA, Hamilton RF. Fabrication of NiTi through additive manufacturing: a review. Prog Mater Sci 2016;83:630–63. https://doi.org/10.1016/j.pmatsci.2016.08.001.
[4] Van Humbeeck J. Additive manufacturing of shape memory alloys. Shape Mem Superelasticity 2018;4:309–12. https://doi.org/10.1007/s40830-018-0174-z.
[5] Wong M, Tsopanos S, Sutcliffe CJ, Owen I. Selective laser melting of heat transfer devices. Rapid Prototyp J 2007;13:291–7. https://doi.org/10.1108/13552540710824797.
[6] Wong M, Owen I, Sutcliffe CJ, Puri A. Convective heat transfer and pressure losses across novel heat sinks fabricated by Selective Laser Melting. Int J Heat Mass Tran 2009;52:281–8. https://doi.org/10.1016/j.ijheatmasstransfer.2008.06.002.
[7] Maskery I, Aremu AO, Simonelli M, Tuck C, Wildman RD, Ashcroft IA, et al. Mechanical properties of Ti-6Al-4V selectively laser melted parts with body-centred-cubic lattices of varying cell size. Exp Mech 2015:1–12. https://doi.org/10.1007/s11340-015-0021-5.
[8] Malukhin K, Ehmann K. Material characterization of NiTi based memory alloys fabricated by the laser direct metal deposition process. J Manuf Sci Eng Trans ASME 2006;128:691–6. https://doi.org/10.1115/1.2193553.
[9] Krishna BV, Bose S, Bandyopadhyay A. Fabrication of porous NiTi shape memory alloy structures using laser engineered net shaping. J Biomed Mater Res B Appl Biomater 2009;89:481–90. https://doi.org/10.1002/jbm.b.31238.
[10] Nishida M, Wayman CM, Honma T. Precipitation processes in near-equiatomic TiNi shape memory alloys. Metall Trans A 1986;17:1505–15. https://doi.org/10.1007/BF02650086.
[11] Abioye TE, Farayibi PK, Kinnel P, Clare AT. Functionally graded Ni-Ti microstructures synthesised in process by direct laser metal deposition. Int J Adv Manuf Technol 2015;79:843–50. https://doi.org/10.1007/s00170-015-6878-8.
[12] Ding D, Pan Z, Cuiuri D, Li H. Wire-feed additive manufacturing of metal components: technologies, developments and future interests. Int J Adv Manuf Technol 2015;81:465–81. https://doi.org/10.1007/s00170-015-7077-3.
[13] Resnina N, Palani IA, Belyaev S, Prabu SSM, Liulchak P, Karaseva U, et al. Structure, martensitic transformations and mechanical behaviour of NiTi shape memory alloy produced by wire arc additive manufacturing. J Alloys Compd 2021;851:156851.
[14] Wang J, Pan Z, Carpenter K, Han J, Wang Z, Li H. Comparative study on crystallographic orientation, precipitation, phase transformation and mechanical response of Ni-rich NiTi alloy fabricated by WAAM at elevated substrate heating temperatures. Mater Sci Eng 2021;800:140307.
[15] Shen C, Reid M, Liss K-D, Hua X, Pan Z, Mou G, et al. In-situ neutron diffraction study on the high temperature thermal phase evolution of wire-arc additively manufactured Ni53Ti47 binary alloy. J Alloys Compd 2020;843:156020.
[16] Wang J, Pan Z, Wang Y, Wang L, Su L, Cuiuri D, et al. Evolution of crystallographic orientation, precipitation, phase transformation and mechanical properties realized by enhancing deposition current for dual-wire arc additive manufactured Ni-rich NiTi alloy. Additive Manufacturing 2020;34:101240.
[17] Zeng Z, Cong BQ, Oliveira JP, Ke WC, Schell N, Peng B, et al. Wire and arc additive manufacturing of a Ni-rich NiTi shape memory alloy: microstructure and mechanical properties. Addit Manuf 2020:32. https://doi.org/10.1016/j.addma.2020.101051.
[18] Demir AG. Micro laser metal wire deposition for additive manufacturing of thin-walled structures. Opt Laser Eng 2018;100. https://doi.org/10.1016/j.optlaseng.2017.07.003.
[19] Demir AG, Biffi CA. Micro laser metal wire deposition of thin-walled Al alloy components: process and material characterization. J Manuf Process 2019;37:362–9. https://doi.org/10.1016/j.jmapro.2018.11.017.
[20] Demir AG. Single track deposition study of biodegradable Mg-rare earth alloy by micro laser metal wire deposition. Mater Today Proc 2019;7:426–34. https://doi.org/10.1016/j.matpr.2018.11.105.
[21] Wanjara P, Brochu M, Jahazi M. Electron beam freeforming of stainless steel using solid wire feed. Mater Des 2007;28:2278–86. https://doi.org/10.1016/j.matdes.2006.08.008.
[22] Abioye TE, Folkes J, Clare AT. A parametric study of Inconel 625 wire laser deposition. J Mater Process Technol 2013;213:2145–51. https://doi.org/10.1016/j.jmatprotec.2013.06.007.
[23] Liu S, Liu W, Harooni M, Ma J, Kovacevic R. Real-time monitoring of laser hot-wire cladding of Inconel 625. Opt Laser Technol 2014;62:124–34. https://doi.org/10.1016/j.optlastec.2014.03.007.
[24] Motta M, Demir AG, Previtali B. High-speed imaging and process characterization of coaxial laser metal wire deposition. Addit Manuf 2018;22:497–507. https://doi.org/10.1016/j.addma.2018.05.043.
[25] Biffi CA, Bassani P, Fiocchi J, Tuissi A. Microstructural and mechanical response of Niti lattice 3D structure produced by selective laser melting. Metals 2020;10:1–9. https://doi.org/10.3390/met10060814 (Basel).
[26] Biffi CA, Fiocchi J, Valenza F, Bassani P, Tuissi A. Selective laser melting of NiTi shape memory alloy: processability, microstructure, and superelasticity. Shape Mem Superelasticity 2020. https://doi.org/10.1007/s40830-020-00298-8.
[27] Khalil-Allafi J, Dlouhy A, Eggeler G. Ni4Ti3-precipitation during aging of NiTi shape memory alloys and its influence on martensitic phase transformations. Acta Mater 2002;50:4255–74. https://doi.org/10.1016/S1359-6454(02)00257-4.
[28] Michutta J, Carroll MC, Yawny A, Somsen C, Neuking K, Eggeler G. Martensitic phase transformation in Ni-rich NiTi single crystals with one family of Ni4Ti3 precipitates. Mater Sci Eng, A 2004;378:152–6. https://doi.org/10.1016/j.msea.2003.11.061.